



1 **Impact of Eastern and Central Pacific El Niño on Lower** 2 **Tropospheric Ozone in China**

3 **Zhongjing Jiang¹, Jing Li¹**

4 ¹ Department of Atmospheric and Oceanic Sciences, School of Physics, Peking University,
5 Beijing, China

6 **Correspondence:** Jing Li (jing-li@pku.edu.cn)

7

8 **Abstract**

9 Tropospheric ozone is an essential atmospheric component as it plays a significant role in
10 influencing radiation equilibrium and ecological health. It is affected not only by anthropogenic
11 activities but also by natural climate variabilities. Here we examine the tropospheric ozone change
12 in China associated with the Eastern Pacific (EP) and Central Pacific (CP) El Niño using satellite
13 observations from 2007 to 2017 and GEOS-Chem simulations from 1980 to 2017. GEOS-Chem
14 simulations reasonably reproduce the satellite-retrieved lower tropospheric ozone (LTO) changes
15 despite a slight underestimation. Results show that El Niño generally exerts negative impacts on
16 LTO concentration in China, except for southeastern China during the pre-CP El Niño autumn and
17 post-EP El Niño summer. The budget analysis further indicates that for both events, LTO changes
18 are dominated by the transport process controlled by circulation patterns and the chemical process
19 influenced by local meteorological anomalies associated with El Niño, especially the solar
20 radiation and relative humidity changes. The differences between EP and CP-induced LTO
21 changes mostly lie in southern China. The different strengths, positions, and duration of western
22 North Pacific anomalous anticyclone (WNPAC) induced by tropical warming are likely



23 responsible for the different EP and CP LTO changes. During the post-EP El Niño summer, the
24 Indian ocean capacitor also plays an important role in controlling LTO changes over southern
25 China.

26 **Key Words**

27 Lower tropospheric ozone, El Niño, meteorological fields, WNPAC, GEOS-Chem

28

29 **1. Introduction**

30 Tropospheric ozone is an important greenhouse gas and a major air pollutant affecting human
31 health and the ecosystem (Fleming et al., 2018; Maji et al., 2019; Mills et al., 2018). Produced
32 from the photochemical oxidation of carbon monoxide (CO) and volatile organic compounds
33 (VOCs) in the presence of nitrogen oxides (NO_x) and sunlight, tropospheric ozone concentration
34 is largely affected by meteorological conditions, including solar radiation, relative humidity,
35 temperature, etc., which can influence the precursor emissions and photochemical reaction rates
36 (Guenther et al., 2012; Jeong et al., 2018). Thus, El Niño-Southern Oscillation (ENSO), as one of
37 the most prominent interannual climate variabilities, can influence ozone concentration by
38 affecting the local meteorological fields and modulating the ozone distribution through changes in
39 atmospheric circulation (Bjerknes, 1969; Chandra et al., 1998; Oman et al., 2013; Sudo and
40 Takahashi, 2001).

41

42 Because ENSO is a tropical signal, the majority of previous studies focus on discussing the impacts
43 of ENSO on tropical tropospheric ozone (Oman et al., 2011; Ziemke et al., 2010; Ziemke and
44 Chandra, 2003). A few studies demonstrated that the influence of ENSO on tropospheric ozone



45 could also extend to subtropics and mid-latitudes. Over Southeast Asia, Marlier et al., (2013) show
46 that during the strong El Niño years, fires contribute up to 50 ppbv in annual average ozone surface
47 concentrations near fire sources. Over the US, Xu et al., (2017) examined the impact of ENSO on
48 ozone during 1993 to 2013 and found that the monthly ozone decreased about 1.8 ppbv per
49 standard deviation of Niño 3.4 index during El Niño years. They found significant spatial
50 dependence and seasonality of ENSO's influence on ozone. ENSO affects surface ozone via
51 different processes during warm or cold seasons in different regions in the US. As for China, a few
52 studies discussed the impact of ENSO on the total column or tropospheric column ozone
53 concentration over part of China, such as Tibet, or include China as part of their study regions
54 (Koumoutsaris et al., 2008; Singh et al., 2002; Xu et al., 2018; Zou et al., 2001). However, studies
55 that specially focused on the influence of ENSO on tropospheric ozone over China are still limited.
56 Yet, ENSO may exert profound impacts on the temperature, precipitation in China both in its
57 developing season and the following year (Cao et al., 2017; Fang et al., 2021; Li et al., 2021, 2018;
58 Xu et al., 2018) and then affect ozone concentrations. In view of the severe ozone pollution in
59 China and the substantial role of natural impacts, it is essential to clarify how ozone concentrations
60 in China respond to ENSO.

61
62 On the other hand, increasing studies have noticed the different flavors of ENSO. A widely
63 accepted view is to categorize El Niño into the Eastern Pacific (EP) and Central Pacific (CP) El
64 Niño (Ashok et al., 2007; Yeh et al., 2009), whose positive sea surface temperature (SST)
65 anomalies are located over the eastern and central Pacific respectively. Whereas previous studies
66 about the response of ozone to ENSO generally used Niño 3.4 index (Olsen et al., 2016; Oman et
67 al., 2013) or the Southern Oscillation index (Koumoutsaris et al., 2008; Ziemke and Chandra,



68 2003) to represent the intensity of ENSO and the difference between the two types of El Niño is
69 neglected. Yet, due to the different generation mechanisms (Yu et al., 2010), the two types of El
70 Niño can induce various changes in climate or synoptic weather in the tropics as well as the mid-
71 to-high latitudes (Shi & Qian, 2018; Yu et al., 2012). Studies have shown that different types of
72 El Niño can induce different changes in tropical cyclone genesis, water vapor transport, and rainfall
73 patterns over China (Feng et al., 2011; Li et al., 2014; Wang and Wang, 2013). As such, they also
74 likely exert different impacts on atmospheric components. Some research explores the
75 teleconnections of different types of El Niño with climate anomalies and haze pollution in China
76 (Gao et al., 2020; Ren et al., 2018; Xu et al., 2018; Yu et al., 2019, 2020), whereas few studies
77 have discussed the teleconnections between ozone and different El Niño types, which is thus the
78 focus of this study.

79

80 In this paper, we investigate the changes of tropospheric ozone in China associated with EP and
81 CP El Niño, using satellite observations and the GEOS-Chem chemistry transport model
82 simulations. This study aims to explore how El Niño influences the lower tropospheric ozone in
83 China to shed light on the ozone air quality control on the interannual timescale. In addition, we
84 hope this study can also improve our understanding of the mechanism of teleconnections between
85 ENSO and tropospheric ozone concentration in mid-latitudes.

86

87 **2. Data and Methods**

88 **2.1 The classification of Eastern and Central Pacific El Niño**

89 To distinguish the type of El Niño, we first used the Oceanic Niño Index (ONI) from the Climate
90 Prediction Center (CPC) of the National Oceanic and Atmospheric Administration (NOAA) to



91 filter out El Niño events. The ONI is defined as the 3-month running mean of ERSST.v5 SST
92 anomalies in the Niño 3.4 region (5°N-5°S, 120°W-170°W), based on centered 30-year base
93 periods updated every five years. An El Niño event is defined as when ONI is greater than or equal
94 to 0.5°C for a period of at least five consecutive overlapping seasons. Then we combined two
95 methods, namely the Niño3/4 method in (Yeh et al., 2009) and the ENSO Modoki index (EMI)
96 method in (Ashok et al., 2007), to discriminate EP and CP El Niño. When the two methods show
97 consensus results, we define it as a typical EP or CP event.

98

99 **Niño3/4 method**

100 We first adopted the same Niño3/4 method in (Yeh et al., 2009). The classification is based on the
101 comparison between boreal winter (DJF) seasonal mean Niño 3 and Niño 4 indices. DJF Niño3
102 SST index is defined as the DJF seasonal SST anomaly in Niño 3 region (150°W-90°W, 5°N-5°S),
103 and DJF Niño 4 SST index is defined as the DJF seasonal SST anomaly in Niño 4 region (160°E-
104 150°W, 5°N-5°S). The first step is to pick out the years when the DJF Niño3 and Niño 4 indices
105 both greater than 0.5°C, then make the comparison between DJF Niño 3 and Niño 4 SST indices.
106 When DJF Niño3 SST index is greater than DJF Niño4 SST index, it is defined as an EP El Niño
107 event, otherwise as a CP El Niño event.

108

109 **El Niño Modoki index (EMI) method**

110 Ashok et al., (2007) derived an El Niño Modoki index (EMI) to capture whether there is a typical
111 CP-type event.

112

$$\text{EMI} = [\text{SSTA}]_A - 0.5 \times [\text{SSTA}]_B - 0.5 \times [\text{SSTA}]_C$$



113 [SSTA]_A, [SSTA]_B, and [SSTA]_C represent the area-averaged SST anomaly of region A (165°E-
114 140°W, 10°S-10°N), B (110°W-70°W, 15°S-5°N), and C (125°E-145°E, 10°S-20°N) respectively.
115 We call a CP El Niño event “typical” when the index amplitude is equal to or greater than 0.7σ ,
116 where σ is the seasonal standard deviation.

117

118 The classification results of EP and CP El Niño of the total 12 events from 1980-2017 are shown
119 in Table 1.

120

121 **2.2 Satellite-retrieved ozone and meteorological data**

122 Ozone abundance in the atmosphere can be measured from space using different remoting-sensing
123 techniques. Frequently used tropospheric column ozone datasets include OMI/MLS carried by
124 AURA and Infrared Atmospheric Sounding Interferometer (IASI) carried by the MetOp satellites.
125 As we prefer to consider lower tropospheric ozone in this study, we choose to use IASI, which can
126 retrieve the ozone from the surface to 6 km. In addition, IASI is also a superior choice considering
127 the spatial coverage, resolution, and data quality. IASI is a thermal infrared Fourier transform
128 spectrometer onboard the MetOp-A and B satellites; as a space-borne nadir-viewing instrument, it
129 probes the troposphere using the thermal infrared spectral range, and the atmospheric data is
130 further retrieved by inversion algorithms (Boynard et al., 2009, 2016). The IASI-A and B
131 instruments have been operationally providing atmospheric products since October 2007 and
132 March 2013, respectively. Ozone monthly gridded data is available on
133 <https://cds.climate.copernicus.eu/cdsapp#!/dataset/satellite-ozone-v1?tab=form>, last access: 8
134 November 2021. We used the ozone data from September 2007 to Autumn 2017, mostly from
135 MetOp-A v0001, with substitutes from MetOp-B v0001 for several missing months in 2015.



136

137 Meteorological fields for 1980-2017 were obtained from the Goddard Earth Observing System
138 (MERRA-2) database (Bosilovich et al., 2016), which is the current operational met data product
139 from the Global Modeling and Assimilation Office (GMAO). The data are available at
140 http://ftp.as.harvard.edu/gcgrid/data/GEOS_2x2.5/MERRA2/, last access: 8 November 2021.
141 Meteorological variables used in section 3.2 include surface downwelling solar radiation (SR),
142 relative humidity (RH), total precipitation (TP), temperature (T), sea level pressure (SLP), and
143 wind fields. RH, T, and winds are multi-level variables. We calculated the 0-6 km column averages
144 to be consistent with ozone, whereas SR, TP, and SLP are single-level variables.

145

146 **2.3 GEOS-Chem simulations**

147 The GEOS-Chem (GC) chemical transport model (Bey et al., 2001; v12.3.2; <http://geos-chem.org>)
148 is used to explore the EP and CP El Niño-related tropospheric ozone changes. We choose the
149 standard chemistry mechanism, which includes both troposphere and stratosphere. The Universal
150 tropospheric-stratospheric Chemistry eXtension (UCX) mechanism developed by Eastham et al.,
151 (2014) combines both tropospheric and stratospheric reactions into a single chemistry mechanism.
152 The model is driven by MERRA-2 meteorological fields with 72 vertical levels and $2^\circ \times 2.5^\circ$
153 horizontal resolution. We first performed a historical run from 1980-2017 with anthropogenic
154 emissions fixed at the year 2000, so the difference among different events is only caused by the
155 meteorological fields. A drawback of this setting is that the biomass burning is also fixed at the
156 year 2000; however, the biogenic emission will still change as it was calculated interactively
157 with meteorology.

158



159 The simulated ozone concentration is further validated against tropospheric ozone within the same
160 altitude range retrieved by the IASI. Because IASI only retrieves column ozone concentration
161 between 0-6 km, our comparison and analysis also focus on 0-6 km integrated column ozone
162 concentration, referred to as lower tropospheric ozone (LTO) thereafter. As satellite observation
163 starts in October 2007, to ensure comparability, we selected the 2015-2016 and 2009-2010 events
164 to represent EP and CP El Niño, respectively. A 10-year average (September 2007-Autumn 2017)
165 was used as the climatological state. Figure S1 shows the seasonal mean SST anomalies for the
166 two periods selected, which corresponds well to EP (2015-2016) and CP (2009-2010) El Niño
167 patterns.

168

169 To further distinguish the ozone changes between EP and CP El Niño, we also performed three
170 composite model simulations driven by the composite meteorological fields for the four seasons
171 of three most typical EP events (1982-1983, 1997-1998, 2015-2016), four CP events (1994-1995,
172 2002-2003, 2004-2005, 2009-2010), and a 30-year averaged climatology (September 1985-
173 Autumn 2015) for comparison. Figure S2 shows the composites of seasonal mean SST anomalies,
174 which well corresponded to EP and CP El Niño.

175

176 Moreover, to explain the physical and chemical drivers of the ozone changes, we analyzed the
177 composite meteorological fields to check the ENSO-related meteorological changes. We also
178 diagnosed the 0-6 km ozone budget changes of different model processes and quantified the
179 absolute contribution of each process. These budget diagnoses are calculated by taking the
180 difference in 0-6 km vertically integrated column ozone mass before and after major GEOS-Chem
181 simulation components, including chemistry, transport, mixing, and convection, at each timestep.



182

183 **3. Results**

184 **3.1 Lower tropospheric ozone changes associated with EP and CP El Niño**

185 An ENSO event usually develops in autumn (SON_0), reaches its peak in winter (DJF_{0-1}), and
186 decays in the following spring (MAM_1) and summer (JJA_1) (Xu et al., 2017). We denote the ENSO
187 developing year as year 0 and the following year as year 1. We first compare the climatology state
188 (Figure S3) between observation and simulation. Model performance is comparable to those in
189 previous modeling works (Dang et al., 2021; Lu et al., 2019; Ni et al., 2018). The bias mainly
190 comes from the resolution, chemical mechanism, microphysics processes, and site
191 representativeness (Sun et al., 2019; Young et al., 2018). Then we examine the change of satellite-
192 retrieved and simulated 0-6 km column ozone during the 2015-2016 EP and 2009-2010 CP events
193 with respect to climatology (Figure 1) to validate the model response to ENSO-related signals.

194

195 EP El Niño generally exerts negative effects on LTO in China in both observation and simulation,
196 except for a dipole mode change over southern China during pre-EP autumn and post-EP summer.
197 The satellite-retrieved LTO shows an increase in the south and a decrease in the north in autumn,
198 while this dipole mode is obscure in the simulation. In winter and spring, both the satellite-
199 retrieved and simulated LTO exhibit coherent decreases over the whole of China, but the intensity
200 in the model is much smaller. In summer, the observation still shows declines over most regions
201 except a slight increase over the southeast coastal area and southwestern China. The simulation
202 shows a similar pattern but with much stronger positive signals over southern China. In contrast,
203 in CP El Niño there are more prominent LTO increases, such as over southern China in autumn,



204 over northeastern China in spring, and over northern China in summer. In autumn, the satellite
205 observation and simulation both exhibit a dipole mode change in the north and south with LTO
206 decrease over northern and increase over southern China. In winter, the observed and simulated
207 LTO shows a reverse change with slightly positive and negative signals. The LTO changes in
208 spring and summer are pretty consistent between observation and simulation.

209

210 In general, the LTO changes are at $-1\sim 1$ DU (Figure S4), accounting for 5~10% of the 0~25 DU
211 mean range. The spatial patterns of the simulated and observed LTO changes agree well, despite
212 an overall underestimation by the model. This underestimation can be explained by the fixed
213 biomass burning emission in the simulation that weakens the sensitivity of tropospheric ozone to
214 ENSO, as this leads to milder changes in ozone precursors such as carbon monoxide. The
215 underestimation in spring and summer is most significant at high latitude areas, such as
216 northeastern China, for both EP and CP events. This deviation probably represents the
217 interferences of other high latitude climate variabilities. Another reason is that the model
218 underestimates the average ozone concentration at high latitudes in winter and spring (Figure S3),
219 probably due to the unprecise halogen chemistry (Wang et al., 2021) and the poor represent of
220 Brewer-Dobson circulation in the model. Thus, the ozone transport from polar regions to northern
221 China can be much less in the model. The overall consistency between simulated and observed
222 LTO changes gives us the confidence to use the model for composite analysis, as the satellite
223 record only covers limited El Niño events.

224

225 To include more El Niño events and check the response of ozone to meteorological fields, we
226 further used the composite meteorological fields of three EP events and four CP events to drive



227 the GEOS-Chem model. Figure 2 shows the LTO changes in China during different seasons of the
228 EP and CP El Niño. It is seen that LTO decreases over most regions in both EP and CP type in the
229 range of 5~10%, whereas only some regional increases are seen in pre- El Niño autumn and post-
230 El Niño summer. LTO decrease consistently during winter and spring, reaching ~10% for western
231 and northern China. It appears that the seasonal alternation of LTO changes in southern China may
232 represent the extension of the remarkable ozone changes over the tropical regions. During the EP
233 (CP) El Niño developing, sustaining, and first decaying periods, there are significant dipolar
234 (tripolar) modes of ozone changes over the tropical Pacific area (Figure S5), which is consistent
235 with the result of previous studies (Chandra et al., 1998; Oman et al., 2013). These ozone changing
236 patterns correspond well with solar radiation changes (Figure S6) since they can modulate the
237 photolysis rates and biogenic emissions. The enhancement of tropospheric ozone production over
238 the west Pacific retreats to lower latitudes in winter and spring when the sun moves to the southern
239 hemisphere; therefore, LTO coherently decreases in China. During winter and spring, the changes
240 associated with CP El Niño are more extensive, spatially uniform, and stronger than EP. For
241 summer, however, EP appears to associate with a more substantial LTO decrease, especially for
242 the northern and southwestern parts. For summer, however, EP appears to associate with a more
243 substantial LTO decrease, especially for the northern and southwestern parts. The region
244 exhibiting the most LTO change differences between EP and CP events is southern China. The
245 differences between EP and CP patterns will be further examined in the next section.

246

247 Because El Niño is generally associated with decreased tropospheric ozone concentration, we also
248 briefly examine the LTO changes during the negative phase, i.e., La Niña events (Figure S7). In
249 contrast to El Niño, La Niña tend to be associated with extensive LTO increases by ~2-5%,



250 especially over northern China, indicating an adverse impact on the already severe tropospheric
251 ozone pollution in this region. An increase in ozone concentration during the post-La Niña spring
252 has also been reported by (Wie et al., 2021). However, because El Niño teleconnections are
253 typically stronger and better established, we still focus on El Niño in this study.

254

255 **3.2 Differences in ozone changes associated with EP and CP El Niño**

256 To clarify the mechanism associated with different LTO changes of the two types of El Niño, we
257 further examine the changes of meteorological variables, including SR, RH, TP, T, SLP, and wind
258 fields during EP (Figure 3) and CP events (Figure 4). The leading two variables impact the local
259 production, and the circulation changes represented by SLP and winds control the regional
260 transport. Although wet scavenging of ozone by TP is insufficient because ozone is insoluble in
261 water, TP is closely related to SR and RH; it is also the primary variable examined to identify
262 ENSO teleconnection. We thus also include TP in the comparison. In addition, we calculate the
263 budget changes corresponding to the EP and CP events from GEOS-Chem simulations. Because
264 chemistry and transport are the two dominant processes accounting for more than 70% of the ozone
265 changes in all conditions (Figure 5), we focus our following discussions on these two processes
266 (Figure 6).

267

268 In the autumn before El Niño, LTO changes for EP type show a general decrease in China (Figure
269 2a), especially in the southeastern part. EP El Niño is always accompanied by an anomalous
270 anticyclone in the Philippine sea (Figure 3q), which produces strong southwestern wind anomalies
271 that transport moisture from the ocean, resulting in increased TP and RH but decreased SR over
272 southeastern China (Figure 3i, e, a). These changes are unfavorable for ozone production but



273 efficient for ozone removal, thus leading to a chemical loss of LTO over southern China (Figure
274 6a). Some regional increase over southwestern China is observed and likely due to the positive
275 contribution of transport (Figure 6e) from India as indicated by the west wind anomalies (Figure
276 3q). During the CP event, there is a moderate dipole mode change (Figure 2e), with decreases in
277 northern China and increases in the southern part. In contrast to EP, an anomalous cyclone appears
278 over the Philippine sea, leading to northwest wind anomalies over southern China that produces a
279 dry condition with increased SR (Figure 4i, e, a). The slight decrease in LTO over northern China
280 is likely attributed to the decreased chemical production (Figure 6i) associated with negative
281 temperature anomalies (Figure 4m), although the signal is not statistically significant. The opposite
282 atmospheric circulation patterns over the Philippian sea during EP and CP events are responses to
283 the different SST anomaly regions under these two conditions, as shown by (Wang and Wang,
284 2013) using simple atmospheric model experiments.

285

286 In winter, when the Pacific SST anomalies reach their maxima, EP and CP El Niño are both
287 associated with increased TP, RH, and decreased SR over southern China (Figure 3b,f,j & 4b,f,j).
288 These similar changes are due to the moisture transport induced by western North Pacific
289 anomalous anticyclones (WNPAC) that occur in both EP and CP El Niño, while EP exhibits greater
290 meteorological changes than CP due to the much stronger anomalous anticyclone (Figure 3r & 4r).
291 As a critical system that links El Niño and East Asia climate change, WNPAC is initiated and
292 maintained by local atmosphere-ocean interaction (Wang et al., 2000) and the moist enthalpy
293 advection/Rossby wave modulation (Wu et al., 2017a, 2017b), the formation and maintenance
294 mechanisms are discussed thoroughly in (Li et al., 2017). Although the meteorological variables
295 change in the same direction, the EP and CP-related LTO changes in winter are still opposite over



296 southern China (Figure 2b&f), where the El Niño teleconnection signal is the most prominent
297 (Wang et al., 2020). Budget analysis reveals that this phenomenon is due to the varying
298 contribution of different model processes. Consistent with the increased RH and decreased SR, the
299 contributions of chemical processes are both negative over this region during EP and CP (Figure
300 6b&j). The southwestern wind anomalies (Figure 3r&4r) bring not only water vapor from the
301 ocean but also ozone from India and China-Indochina Peninsula to southern China, contributing
302 to LTO concentration there. During EP, the chemical loss (Figure 6b) exceeds the positive
303 transport (Figure 6f) due to the severe change of SR and RH over southern China (Figure 3b&f).
304 However, for CP conditions, the chemical loss (Figure 6j) due to the increased RH is much weaker
305 and is offset or even exceeded by transport (Figure 6n). This is also consistent with the much larger
306 absolute contribution of transport than chemistry for CP (Figure 5f).

307

308 In spring, LTO decreases extensively over entire northern China under both EP and CP conditions
309 (Figure 2c&g), coherent with the large-scale reduction of SR and increase of RH (Figure 3c,g
310 &4c,g). WNPAC maintains under EP conditions according to the moist enthalpy advection
311 mechanism (Wu et al., 2017a), whereas it nearly disappears in CP (Feng et al., 2011). In EP
312 condition, with the slight westward shift of the anticyclone center from winter to spring, the wind
313 anomalies also shift from southwesterly to southerly, bringing more moisture, and further
314 enhancing TP in higher latitudes where RH increases and SR decreases coherently. However, the
315 chemistry still contributes positively over eastern China (Figure 6c), which might be attributed to
316 the increased temperature related to the warm south winds (Figure 3o&s). As the climate warms
317 from winter to spring, the role of temperature becomes increasingly important. However, as the
318 southerlies blow low ozone air from the ocean, the severe negative transport (Figure 6g) dominates



319 the overall ozone decrease. In CP, however, regional transport is weaker due to the unremarkable
320 change of circulation patterns over the western north Pacific compared to the EP condition; thus,
321 the absolute contribution of transport and chemistry are comparable for CP (Figure 5g).

322

323 The situation for the post-El Niño summer is more complicated as El Niño teleconnections
324 substantially involve air-sea interactions and inter-basin teleconnections (Feng et al., 2011; Kug et
325 al., 2009). Ozone changes for the EP condition show a decrease over central and northern China
326 and a band-like ozone increase over southeastern China (Figure 2d). Although the chemical
327 production (Figure 6d) increases with the slight SR increase and RH decrease (Figure 3d&h) over
328 China's eastern coastal line, the transport process (Figure 6h) controlled by southwestern wind
329 anomalies dominates the ozone decline over the Yangtze river basin and increases over the
330 southeastern coastal line. The circulation anomalies manifest as a tripolar pattern with an
331 anomalous anti-cyclone (AAC) over the southern China sea and an anomalous cyclone circulation
332 (ACC) over Japan (Figure 3t). This pattern appears to be induced by the Indian Ocean capacitor
333 (IOC) effect, which indicates the Indian Ocean (IO) memory of ENSO influence (Chen et al., 2012;
334 Xie et al., 2009; Yang et al., 2007). Since the convection is suppressed in the AAC, the drier
335 condition corresponds well with the positive LTO changes over the Philippine sea (Figure S5d).
336 This positive signal extends to southeastern China coastal areas due to the transport by the
337 southwest wind anomalies. During CP, ozone decreases coherently over most of China (Figure
338 2h). As no significant IO warming appears (Figure S2h), the summer climate is influenced more
339 by the western Pacific warm pool. The negative SST anomalies in the central-east Pacific imply
340 an upcoming La Niña. Accordingly, the western Pacific warm pool begins to shrink with the
341 building of La Niña (Johnson and Birnbaum, 2017). Associated with the SST drop, SLP increases



342 over the northwestern Pacific (Figure 4t), resulting in an enhanced western Pacific subtropical high
343 (WPSH), which is a typical feature of CP El Niño (Chen et al., 2019). Controlled more by local
344 Pacific than IO, the SLP center shifts eastward compared to AAC in EP, and the positive LTO
345 anomalies also move eastward accordingly (Figure S5h). Regional transport (Figure 6g) by the
346 southwest wind anomalies surrounding the positive SLP center exerts a consistent negative
347 contribution to LTO in southern China (Figure 2h; Jiang et al., 2021). In sum, the post-El Niño
348 summer LTO change is dominated by the IOC effect for EP and WPSH enhancement for CP.

349

350 4. Conclusions and discussions

351 This study investigates the changes in tropospheric ozone concentration in China associated with
352 the EP and CP El Niño using satellite observations and GEOS-Chem chemical transport model
353 simulations. The general consistency between observed and simulated results confirms the model's
354 credibility. Overall, both types of El Niño exert a negative effect on LTO by 5~10%, with some
355 regional increases. The ozone changes were explained from the perspective of El Niño-induced
356 meteorological fields, which further lead to changes in local production, regional transport, etc.
357 Budget analysis indicates transport controlled by circulation patterns plays the leading role, and
358 chemistry affected by SR and RH plays the second role in driving the ozone changes. The
359 difference between EP and CP mainly lies in southern China. During the autumn, LTO decreases
360 (increases) about 4~8% (+2~4%) over southern China for EP (CP) type, corresponding well to
361 reversed changes of TP and related variables controlled by the different locations of SST
362 anomalies. In winter, the formed WNPAC maintains during both EP and CP, exerting a
363 counteracting effect on local production and regional transport. The impact of chemistry outweighs
364 the transport for EP, resulting in a slight LTO decrease over southern China (4~6%), vice versa



365 for CP (+0~2%). In spring, the WNPAC persisted under EP condition keeps exerting on ozone and
366 the transport dominates the overall decline of LTO for 5~10%, as the WNPAC disappeared in CP,
367 the role of transport weakens and the drier environment contributes to local production, which
368 leads to a slight ozone increase (+0~4%) over southern China. As for summer, the LTO decreases
369 5~10% in both types except for an increase over the southeastern coastal line for EP. Ozone
370 changes in EP type are dominated by the Indian ocean capacitor, and CP type are influenced more
371 by WPSH.

372

373 Our study indicates that natural variability, such as ENSO, can significantly impact lower
374 tropospheric ozone in mid to high latitudes. This has particular implications for ozone pollution
375 control in China. As much efforts have been taken to control anthropogenic emissions,
376 meteorological factors may play an increasingly important role in the future. The occurrence of El
377 Niño events produces a favorable environment for ozone pollution control in general, but caution
378 needs to be taken for southern China during CP autumn and EP summer. By contrast, when a La
379 Niña is predicted to occur, more strict emission control measures should be taken in the following
380 seasons, especially for northern China. Furthermore, by exploring the association between
381 different ENSO flavors and lower tropospheric ozone in China, this study enriches the theory of
382 ENSO teleconnection in mid-latitudes.

383

384 Nonetheless, there are still limitations in the current study that are subject to future improvements.
385 Tropospheric ozone concentration is influenced by stratospheric-tropospheric exchange (STE)
386 (Ding and Wang, 2006; Langford, 1999), although the effect is primarily concentrated in the upper
387 troposphere(Lin et al., 2015; Neu et al., 2014). Future work is needed to explain the difference of



388 ozone concentration in the vertical dimension and quantify the role of STE in the ENSO-induced
389 LTO changes. The role of biomass burning emission, which also varies with ENSO, will also be
390 investigated. Furthermore, long-term observations, especially in China, are needed to verify the
391 model results reported here.

392

393

394 **Code and data availability.** The IASI satellite tropospheric column ozone data are available on
395 <https://cds.climate.copernicus.eu/cdsapp#!/dataset/satellite-ozone-v1?tab=form>,
396 doi:10.24381/cds.4ebfe4eb, last access: 8 November 2021. The MERRA2 meteorology data is
397 available at http://ftp.as.harvard.edu/gcgrid/data/GEOS_2x2.5/MERRA2/, last access: 8
398 November 2021 (Bosilovich et al., 2016). The GEOS-Chem model is a community model and is
399 freely available (http://wiki.seas.harvard.edu/geos-chem/index.php/GEOS-Chem_12#12.3.2,
400 doi:10.5281/zenodo.2658178, Yantosca, 2019).

401

402

403 **Author contributions.** JL and ZJ designed the study. ZJ ran the GEOS-Chem model and
404 performed the analysis. ZJ and JL wrote the paper.

405

406 **Competing interests.** The authors declare that they have no conflict of interest.

407

408 **Acknowledgments.** We appreciate GMAO for providing the MERRA-2 meteorological data. We
409 thank ECMWF for providing the ozone monthly gridded data. We also acknowledge the efforts of
410 the GEOS-Chem Working Groups and Support Team for developing and maintaining the GEOS-
411 Chem model.

412

413 **Financial support.** This study is funded by the National Natural Science Foundation of China
414 (NSFC) Grant No. 41975023.

415



416 **References**

- 417 Ashok, K., Behera, S. K., Rao, S. A., Weng, H. and Yamagata, T.: El Niño Modoki and its possible
418 teleconnection, *J. Geophys. Res. Ocean.*, 112(11), 1–27, doi:10.1029/2006JC003798, 2007.
- 419 Bey, I., Jacob, D. J., Yantosca, R. M., Logan, J. A., Field, B. D., Fiore, A. M., Li, Q., Liu, H. Y.,
420 Mickley, L. J. and Schultz, M. G.: Global modeling of tropospheric chemistry with
421 assimilated meteorology: Model description and evaluation, *J. Geophys. Res. Atmos.*,
422 106(D19), 23073–23095, doi:10.1029/2001JD000807, 2001.
- 423 Bosilovich, M. G., R. Lucchesi, and M. Suarez, 2016: MERRA-2: File Specification. GMAO
424 Office Note No. 9 (Version 1.1), 73 pp, available from
425 http://gmao.gsfc.nasa.gov/pubs/office_notes.
- 426 Bjerknes, J.: Atmospheric Teleconnections From the Equatorial Pacific, *Mon. Weather Rev.*,
427 97(3), 163–172 [online] Available from: [http://journals.ametsoc.org/doi/abs/10.1175/1520-0493\(1969\)097%3C0163:ATFTEP%3E2.3.CO;2](http://journals.ametsoc.org/doi/abs/10.1175/1520-0493(1969)097%3C0163:ATFTEP%3E2.3.CO;2), 1969.
- 429 Boynard, A., Clerbaux, C., Coheur, P. F., Hurtmans, D., Turquety, S., George, M., Hadji-Lazaro,
430 J., Keim, C. and Meyer-Arnek, J.: Measurements of total and tropospheric ozone from IASI:
431 Comparison with correlative satellite, ground-based and ozonesonde observations, *Atmos.*
432 *Chem. Phys.*, 9(16), 6255–6271, doi:10.5194/acp-9-6255-2009, 2009.
- 433 Boynard, A., Hurtmans, D., Koukouli, M. E., Goutail, F., Bureau, J., Safieddine, S., Lerot, C.,
434 Hadji-Lazaro, J., Wespes, C., Pommereau, J. P., Pazmino, A., Zyrichidou, I., Balis, D., Barbe,
435 A., Mikhailenko, S. N., Loyola, D., Valks, P., Van Roozendaal, M., Coheur, P. F. and
436 Clerbaux, C.: Seven years of IASI ozone retrievals from FORLI: Validation with independent
437 total column and vertical profile measurements, *Atmos. Meas. Tech.*, 9(9), 4327–4353,
438 doi:10.5194/amt-9-4327-2016, 2016.
- 439 Cao, Q., Hao, Z., Yuan, F., Su, Z., Berndtsson, R., Hao, J. and Nyima, T.: Impact of ENSO regimes
440 on developing- and decaying-phase precipitation during rainy season in China, *Hydrol. Earth*
441 *Syst. Sci.*, 21(11), 5415–5426, doi:10.5194/hess-21-5415-2017, 2017.
- 442 Chandra, S., Ziemke, J. R., Min, W. and Read, W. G.: Effects of 1997-1998 El Niño on
443 tropospheric ozone and water vapor, *Geophys. Res. Lett.*, 25(20), 3867–3870,
444 doi:10.1029/98GL02695, 1998.
- 445 Chen, M., Yu, J. Y., Wang, X. and Jiang, W.: The Changing Impact Mechanisms of a Diverse El
446 Niño on the Western Pacific Subtropical High, *Geophys. Res. Lett.*, 46(2), 953–962,



- 447 doi:10.1029/2018GL081131, 2019.
- 448 Chen, W., Park, J. K., Dong, B., Lu, R. and Jung, W. S.: The relationship between El Niño and the
449 western North Pacific summer climate in a coupled GCM: Role of the transition of El Niño
450 decaying phases, *J. Geophys. Res. Atmos.*, 117(12), doi:10.1029/2011JD017385, 2012.
- 451 Dang, R., Liao, H. and Fu, Y.: Quantifying the anthropogenic and meteorological influences on
452 summertime surface ozone in China over 2012–2017, *Sci. Total Environ.*, 754,
453 doi:10.1016/j.scitotenv.2020.142394, 2021.
- 454 Ding, A. and Wang, T.: Influence of stratosphere-to-troposphere exchange on the seasonal cycle of
455 surface ozone at Mount Waliguan in western China, *Geophys. Res. Lett.*, 33(3), 4–7,
456 doi:10.1029/2005GL024760, 2006.
- 457 Eastham, S. D., Weisenstein, D. K. and Barrett, S. R. H.: Development and evaluation of the
458 unified tropospheric-stratospheric chemistry extension (UCX) for the global chemistry-
459 transport model GEOS-Chem, *Atmos. Environ.*, 89, 52–63,
460 doi:10.1016/j.atmosenv.2014.02.001, 2014.
- 461 Fang, K., Yao, Q., Guo, Z., Zheng, B., Du, J., Qi, F., Yan, P., Li, J., Ou, T., Liu, J., He, M. and
462 Trouet, V.: ENSO modulates wildfire activity in China, *Nat. Commun.*, 12(1), 1–8,
463 doi:10.1038/s41467-021-21988-6, 2021.
- 464 Feng, J., Chen, W., Tam, C. Y. and Zhou, W.: Different impacts of El Niño and El Niño Modoki
465 on China rainfall in the decaying phases, *Int. J. Climatol.*, 31(14), 2091–2101,
466 doi:10.1002/joc.2217, 2011.
- 467 Fleming, Z. L., Doherty, R. M., Von Schneidmesser, E., Malley, C. S., Cooper, O. R., Pinto, J.
468 P., Colette, A., Xu, X., Simpson, D., Schultz, M. G., Lefohn, A. S., Hamad, S., Moolla, R.,
469 Solberg, S. and Feng, Z.: Tropospheric Ozone Assessment Report: Present-day ozone
470 distribution and trends relevant to human health, *Elementa*, 6, doi:10.1525/elementa.273,
471 2018.
- 472 Gao, T., Luo, M., Lau, N. C. and Chan, T. O.: Spatially Distinct Effects of Two El Niño Types on
473 Summer Heat Extremes in China, *Geophys. Res. Lett.*, 47(6), 1–9,
474 doi:10.1029/2020GL086982, 2020.
- 475 Guenther, A. B., Jiang, X., Heald, C. L., Sakulyanontvittaya, T., Duhl, T., Emmons, L. K. and
476 Wang, X.: The model of emissions of gases and aerosols from nature version 2.1
477 (MEGAN2.1): An extended and updated framework for modeling biogenic emissions,



- 478 Geosci. Model Dev., 5(6), 1471–1492, doi:10.5194/gmd-5-1471-2012, 2012.
- 479 Jeong, J. I., Park, R. J. and Yeh, S. W.: Dissimilar effects of two El Niño types on PM2.5
480 concentrations in East Asia, Environ. Pollut., 242, 1395–1403,
481 doi:10.1016/j.envpol.2018.08.031, 2018.
- 482 Jiang, Z., Li, J., Lu, X., Gong, C., Zhang, L. and Liao, H.: Impact of Western Pacific Subtropical
483 High on Ozone Pollution over Eastern China, Atmos. Chem. Phys., 1–37, doi:10.5194/acp-
484 2020-646, 2021.
- 485 Johnson, G. C. and Birnbaum, A. N.: As El Niño builds, Pacific Warm Pool expands, ocean gains
486 more heat, Geophys. Res. Lett., 44(1), 438–445, doi:10.1002/2016GL071767, 2017.
- 487 Koumoutsaris, S., Bey, I., Generoso, S. and Thouret, V.: Influence of El Niño–Southern Oscillation
488 on the interannual variability of tropospheric ozone in the northern midlatitudes, J. Geophys.
489 Res. Atmos., 113(19), 1–21, doi:10.1029/2007JD009753, 2008.
- 490 Kug, J. S., Jin, F. F. and An, S. II: Two types of El Niño events: Cold tongue El Niño and warm
491 pool El Niño, J. Clim., 22(6), 1499–1515, doi:10.1175/2008JCLI2624.1, 2009.
- 492 Langford, A. O.: Stratosphere-troposphere exchange at the subtropical jet: Contribution to the
493 tropospheric ozone budget at midlatitudes, Geophys. Res. Lett., 26(16), 2449–2452,
494 doi:10.1029/1999GL900556, 1999.
- 495 Li, H., Fan, K., He, S., Liu, Y., Yuan, X. and Wang, H.: Intensified impacts of central pacific
496 ENSO on the reversal of December and January surface air temperature anomaly over China
497 since 1997, J. Clim., 34(5), 1601–1618, doi:10.1175/JCLI-D-20-0048.1, 2021.
- 498 Li, J., Huang, D., Li, F. and Wen, Z.: Circulation characteristics of EP and CP ENSO and their
499 impacts on precipitation in South China, J. Atmos. Solar-Terrestrial Phys., 179(January),
500 405–415, doi:10.1016/j.jastp.2018.09.006, 2018.
- 501 Li, T., Wang, B., Wu, B., Zhou, T., Chang, C. P. and Zhang, R.: Theories on formation of an
502 anomalous anticyclone in western North Pacific during El Niño: A review, J. Meteorol. Res.,
503 31(6), 987–1006, doi:10.1007/s13351-017-7147-6, 2017.
- 504 Li, X., Zhou, W., Chen, D., Li, C. and Song, J.: Water vapor transport and moisture budget over
505 eastern China: Remote forcing from the two types of El Niño, J. Clim., 27(23), 8778–8792,
506 doi:10.1175/JCLI-D-14-00049.1, 2014.
- 507 Lin, M., Fiore, A. M., Horowitz, L. W., Langford, A. O., Oltmans, S. J., Tarasick, D. and Rieder,
508 H. E.: Climate variability modulates western US ozone air quality in spring via deep



- 509 stratospheric intrusions, *Nat. Commun.*, 6(May), 1–11, doi:10.1038/ncomms8105, 2015.
- 510 Lu, X., Zhang, L., Chen, Y., Zhou, M., Zheng, B., Li, K., Liu, Y., Lin, J., Fu, T. M. and Zhang,
511 Q.: Exploring 2016–2017 surface ozone pollution over China: Source contributions and
512 meteorological influences, *Atmos. Chem. Phys.*, 19(12), 8339–8361, doi:10.5194/acp-19-
513 8339-2019, 2019.
- 514 Maji, K. J., Ye, W. F., Arora, M. and Nagendra, S. M. S.: Ozone pollution in Chinese cities:
515 Assessment of seasonal variation, health effects and economic burden, *Environ. Pollut.*,
516 247(x), 792–801, doi:10.1016/j.envpol.2019.01.049, 2019.
- 517 Marlier, M. E., Defries, R. S., Voulgarakis, A., Kinney, P. L., Randerson, J. T., Shindell, D. T.,
518 Chen, Y. and Faluvegi, G.: El Niño and health risks from landscape fire emissions in southeast
519 Asia, *Nat. Clim. Chang.*, 3(2), 131–136, doi:10.1038/nclimate1658, 2013.
- 520 Mills, G., Pleijel, H., Malley, C. S., Sinha, B., Cooper, O. R., Schultz, M. G., Neufeld, H. S.,
521 Simpson, D., Sharps, K., Feng, Z., Gerosa, G., Harmens, H., Kobayashi, K., Saxena, P.,
522 Paoletti, E., Sinha, V. and Xu, X.: Tropospheric Ozone Assessment Report: Present-day
523 tropospheric ozone distribution and trends relevant to vegetation, edited by D. Helmig and A.
524 Lewis, *Elem. Sci. Anthr.*, 6, doi:10.1525/elementa.302, 2018.
- 525 Neu, J. L., Flury, T., Manney, G. L., Santee, M. L., Livesey, N. J. and Worden, J.: Tropospheric
526 ozone variations governed by changes in stratospheric circulation, *Nat. Geosci.*, 7(5), 340–
527 344, doi:10.1038/ngeo2138, 2014.
- 528 Ni, R., Lin, J., Yan, Y., Lin, W. and Chen, H.: Foreign and Domestic Contributions to Springtime
529 Anthropogenic Ozone Pollution over China Severe Ozone Pollution in China, *Atmos. Chem.*
530 *Phys.*, 18, 11447–11469, 2018.
- 531 Olsen, M. A., Wargan, K. and Pawson, S.: Tropospheric column ozone response to ENSO in
532 GEOS-5 assimilation of OMI and MLS ozone data, *Atmos. Chem. Phys.*, 16(11), 7091–7103,
533 doi:10.5194/acp-16-7091-2016, 2016.
- 534 Oman, L. D., Ziemke, J. R., Douglass, A. R., Waugh, D. W., Lang, C., Rodriguez, J. M. and
535 Nielsen, J. E.: The response of tropical tropospheric ozone to ENSO, *Geophys. Res. Lett.*,
536 38(13), 2–7, doi:10.1029/2011GL047865, 2011.
- 537 Oman, L. D., Douglass, A. R., Ziemke, J. R., Rodriguez, J. M., Waugh, D. W. and Nielsen, J. E.:
538 The ozone response to enso in aura satellite measurements and a chemistry-climate
539 simulation, *J. Geophys. Res. Atmos.*, 118(2), 965–976, doi:10.1029/2012JD018546, 2013.



- 540 Ren, H. L., Lu, B., Wan, J., Tian, B. and Zhang, P.: Identification Standard for ENSO Events and
541 Its Application to Climate Monitoring and Prediction in China, *J. Meteorol. Res.*, 32(6), 923–
542 936, doi:10.1007/s13351-018-8078-6, 2018.
- 543 Shi, J. and Qian, W.: Asymmetry of two types of ENSO in the transition between the East Asian
544 winter monsoon and the ensuing summer monsoon, *Clim. Dyn.*, 51(9–10), 3907–3926,
545 doi:10.1007/s00382-018-4119-1, 2018.
- 546 Singh, R. P., Sarkar, S. and Singh, A.: Effect of El Niño on inter-annual variability of ozone during
547 the period 1978–2000 over the Indian subcontinent and China, *Int. J. Remote Sens.*, 23(12),
548 2449–2456, doi:10.1080/01431160110075893, 2002.
- 549 Sudo, K. and Takahashi, M.: Simulation of tropospheric ozone changes during 1997–1998 El Niño:
550 Meteorological impact on tropospheric photochemistry, *Geophys. Res. Lett.*, 28(21), 4091–
551 4094, doi:10.1029/2001GL013335, 2001.
- 552 Sun, L., Xue, L., Wang, Y., Li, L., Lin, J., Ni, R., Yan, Y., Chen, L., Li, J., Zhang, Q. and Wang,
553 W.: Impacts of meteorology and emissions on summertime surface ozone increases over
554 central eastern China between 2003 and 2015, *Atmos. Chem. Phys.*, 19(3), 1455–1469,
555 doi:10.5194/acp-19-1455-2019, 2019.
- 556 Wang, B., Wu, R. and Fu, X.: Pacific-East Asian teleconnection: How does ENSO affect East
557 Asian climate?, *J. Clim.*, 13(9), 1517–1536, doi:10.1175/1520-
558 0442(2000)013<1517:PEATHD>2.0.CO;2, 2000.
- 559 Wang, B., Luo, X. and Liu, J.: How robust is the asian precipitation-ENSO relationship during the
560 industrial warming period (1901–2017)?, *J. Clim.*, 33(7), 2779–2792, doi:10.1175/JCLI-D-
561 19-0630.1, 2020.
- 562 Wang, C. and Wang, X.: Classifying el niño modoki I and II by different impacts on rainfall in
563 southern China and typhoon tracks, *J. Clim.*, 26(4), 1322–1338, doi:10.1175/JCLI-D-12-
564 00107.1, 2013.
- 565 Wang, X., Jacob, D. J., Downs, W., Zhai, S., Zhu, L., Shah, V., Holmes, C. D., Sherwen, T.,
566 Alexander, B., Evans, M. J., Eastham, S. D., Neuman, J. A., Veres, P. R., Koenig, T. K.,
567 Volkamer, R., Huey, L. G., Bannan, T. J., Percival, C. J., Lee, B. H., and Thornton, J. A.:
568 Global tropospheric halogen (Cl, Br, I) chemistry and its impact on oxidants, *Atmos. Chem.*
569 *Phys.*, 21, 13973–13996, doi:10.5194/acp-21-13973-2021, 2021.
- 570 Wie, J., Moon, B., Yeh, S., Park, R. J., Kim, B., La Niña-related tropospheric column ozone



- 571 enhancement over East Asia, *Atmos. Environ.*, 261(October 2020), 118575,
572 doi:10.1016/j.atmosenv.2021.118575, 2021.
- 573 Wu, B., Zhou, T. and Li, T.: Atmospheric dynamic and thermodynamic processes driving the
574 western North Pacific anomalous anticyclone during El Niño. Part I: Maintenance
575 mechanisms, *J. Clim.*, 30(23), 9621–9635, doi:10.1175/JCLI-D-16-0489.1, 2017a.
- 576 Wu, B., Zhou, T. and Li, T.: Atmospheric dynamic and thermodynamic processes driving the
577 western north Pacific anomalous anticyclone during El Niño. Part II: Formation processes, *J.*
578 *Clim.*, 30(23), 9637–9650, doi:10.1175/JCLI-D-16-0495.1, 2017b.
- 579 Xie, S. P., Hu, K., Hafner, J., Tokinaga, H., Du, Y., Huang, G. and Sampe, T.: Indian Ocean
580 capacitor effect on Indo-Western pacific climate during the summer following El Niño, *J.*
581 *Clim.*, 22(3), 730–747, doi:10.1175/2008JCLI2544.1, 2009.
- 582 Xu, K., Huang, Q.-L., Tam, C.-Y., Wang, W., Chen, S. and Zhu, C.: Roles of tropical SST patterns
583 during two types of ENSO in modulating wintertime rainfall over southern China, *Clim. Dyn.*,
584 doi:10.1007/s00382-018-4170-y, 2018.
- 585 Xu, L., Yu, J. Y., Schnell, J. L. and Prather, M. J.: The seasonality and geographic dependence of
586 ENSO impacts on U.S. surface ozone variability, *Geophys. Res. Lett.*, 44(7), 3420–3428,
587 doi:10.1002/2017GL073044, 2017.
- 588 Yang, J., Liu, Q., Xie, S. P., Liu, Z. and Wu, L.: Impact of the Indian Ocean SST basin mode on
589 the Asian summer monsoon, *Geophys. Res. Lett.*, 34(2), 1–5, doi:10.1029/2006GL028571,
590 2007.
- 591 Yantosca, B.: geoschem/geos-chem: GEOS-Chem 12.3.2 (Version12.3.2), Zenodo,
592 doi:/10.5281/zenodo.2658178, 2019.
- 593 Yeh, S. W., Kug, J. S., Dewitte, B., Kwon, M. H., Kirtman, B. P. and Jin, F. F.: El Niño in a
594 changing climate, *Nature*, 461(7263), 511–514, doi:10.1038/nature08316, 2009.
- 595 Young, P. J., Naik, V., Fiore, A. M., Gaudel, A., Guo, J., Lin, M. Y., Neu, J. L., Parrish, D. D.,
596 Rieder, H. E., Schnell, J. L., Tilmes, S., Wild, O., Zhang, L., Ziemke, J., Brandt, J., Delcloo,
597 A., Doherty, R. M., Geels, C., Hegglin, M. I., Hu, L., Im, U., Kumar, R., Luhar, A., Murray,
598 L., Plummer, D., Rodriguez, J., Saiz-Lopez, A., Schultz, M. G., Woodhouse, M. T. and Zeng,
599 G.: Tropospheric ozone assessment report: Assessment of global-scale model performance
600 for global and regional ozone distributions, variability, and trends, *Elementa*, 6,
601 doi:10.1525/elementa.265, 2018.



- 602 Yu, J. Y., Kao, H. Y. and Lee, T.: Subtropics-related interannual sea surface temperature
603 variability in the central equatorial pacific, *J. Clim.*, 23(11), 2869–2884,
604 doi:10.1175/2010JCLI3171.1, 2010.
- 605 Yu, J. Y., Zou, Y., Kim, S. T. and Lee, T.: The changing impact of El Niño on US winter
606 temperatures, *Geophys. Res. Lett.*, 39(15), doi:10.1029/2012GL052483, 2012.
- 607 Yu, X., Wang, Z., Zhang, H. and Zhao, S.: Impacts of different types and intensities of El Niño
608 events on winter aerosols over China, *Sci. Total Environ.*, 655, 766–780,
609 doi:10.1016/j.scitotenv.2018.11.090, 2019.
- 610 Yu, X., Wang, Z., Zhang, H., He, J. and Li, Y.: Contrasting impacts of two types of El Niño events
611 on winter haze days in China’s Jing-Jin-Ji region, *Atmos. Chem. Phys.*, 20(17), 10279–10293,
612 doi:10.5194/acp-20-10279-2020, 2020.
- 613 Ziemke, J. R. and Chandra, S.: La Nina and El Nino - Induced variabilities of ozone in the tropical
614 lower atmosphere during 1970-2001, *Geophys. Res. Lett.*, 30(3), 30–33,
615 doi:10.1029/2002GL016387, 2003.
- 616 Ziemke, J. R., Chandra, S., Oman, L. D. and Bhartia, P. K.: A new ENSO index derived from
617 satellite measurements of column ozone, *Atmos. Chem. Phys.*, 10(8), 3711–3721,
618 doi:10.5194/acp-10-3711-2010, 2010.
- 619 Zou, H., Ji, C., Zhou, L., Wang, W. and Jian, Y.: ENSO signal in total ozone over Tibet, *Adv.*
620 *Atmos. Sci.* 18(2), 231–238 (2001). doi:10.1007/s00376-001-0016-2, 2001.
- 621
- 622

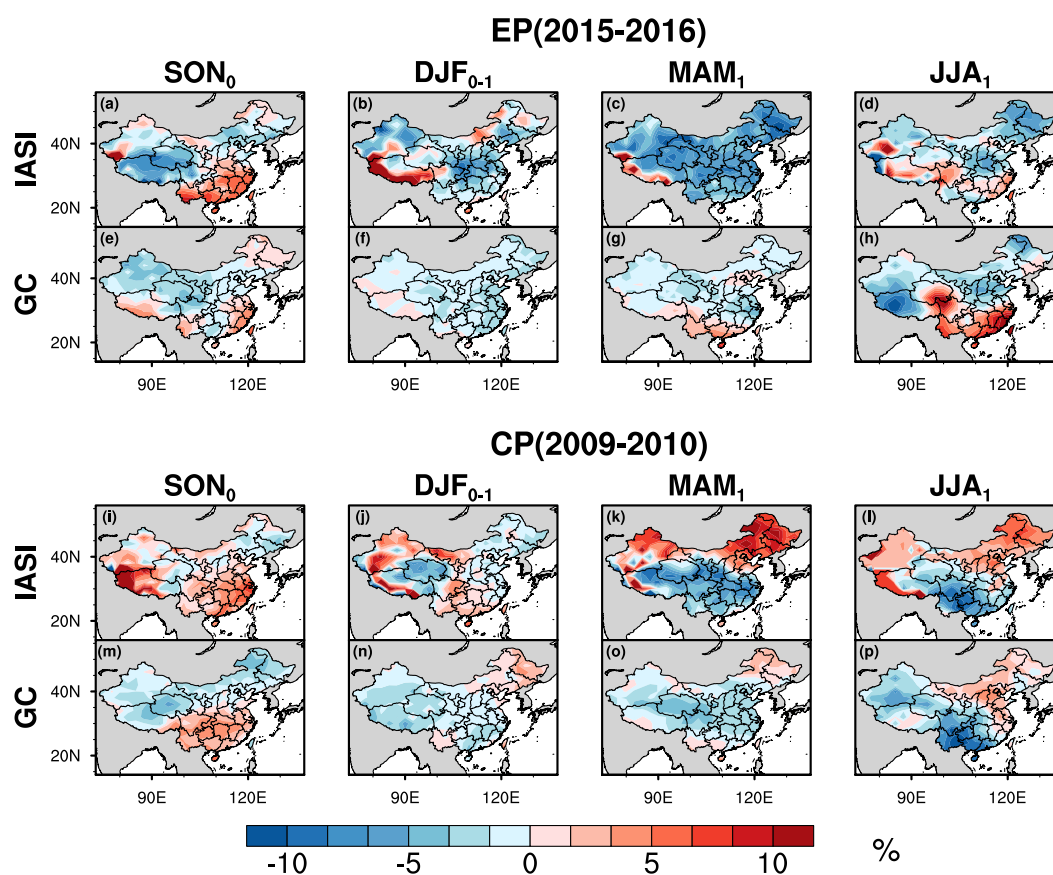


Figure 1. The percentage changes (unit: %) of satellite-observed (IASI) and model-simulated (GC) tropospheric column ozone (0-6 km, unit: DU) for four seasons in EP (2015-2016) and CP (2009-2010) El Niño years.

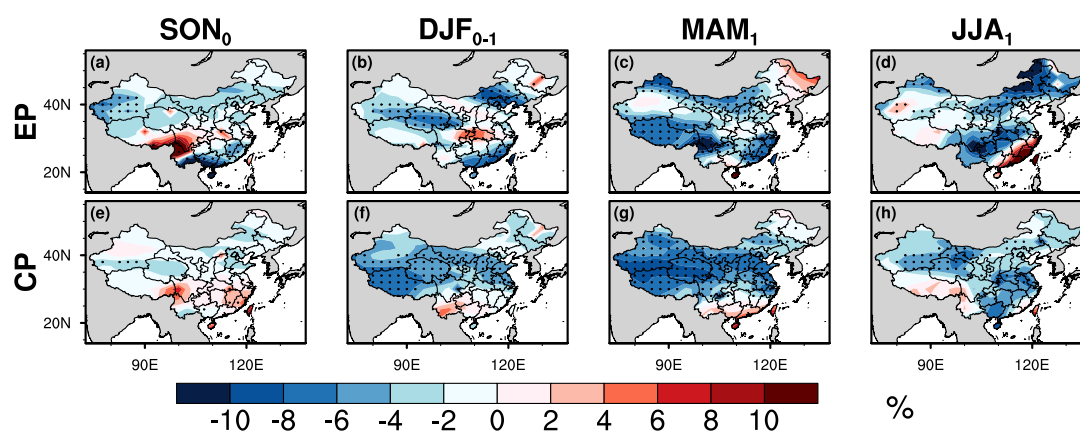


Figure 2. The percentage changes (unit: %) of simulated (GC) tropospheric column ozone (0-6 km, unit: DU) anomalies driven by composite meteorological fields for four seasons in EP and CP El Niño years. Black dots represent the 95% confidence level by t-test.

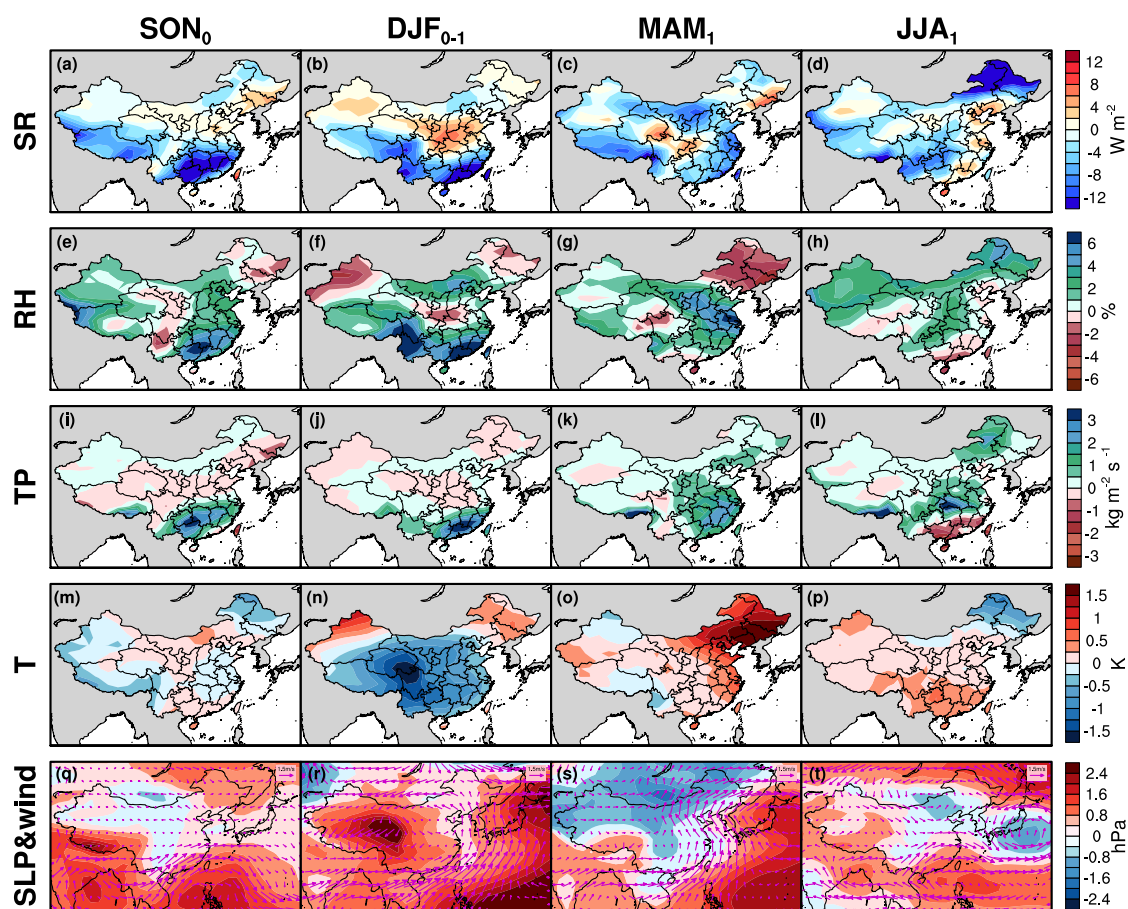


Figure 3. The composite anomalies of meteorological variables, including surface downwelling solar radiation (SR), relative humidity (RH), total precipitation (TP), temperature (T), sea level pressure (SLP), and winds, for four seasons in EP El Niño years.

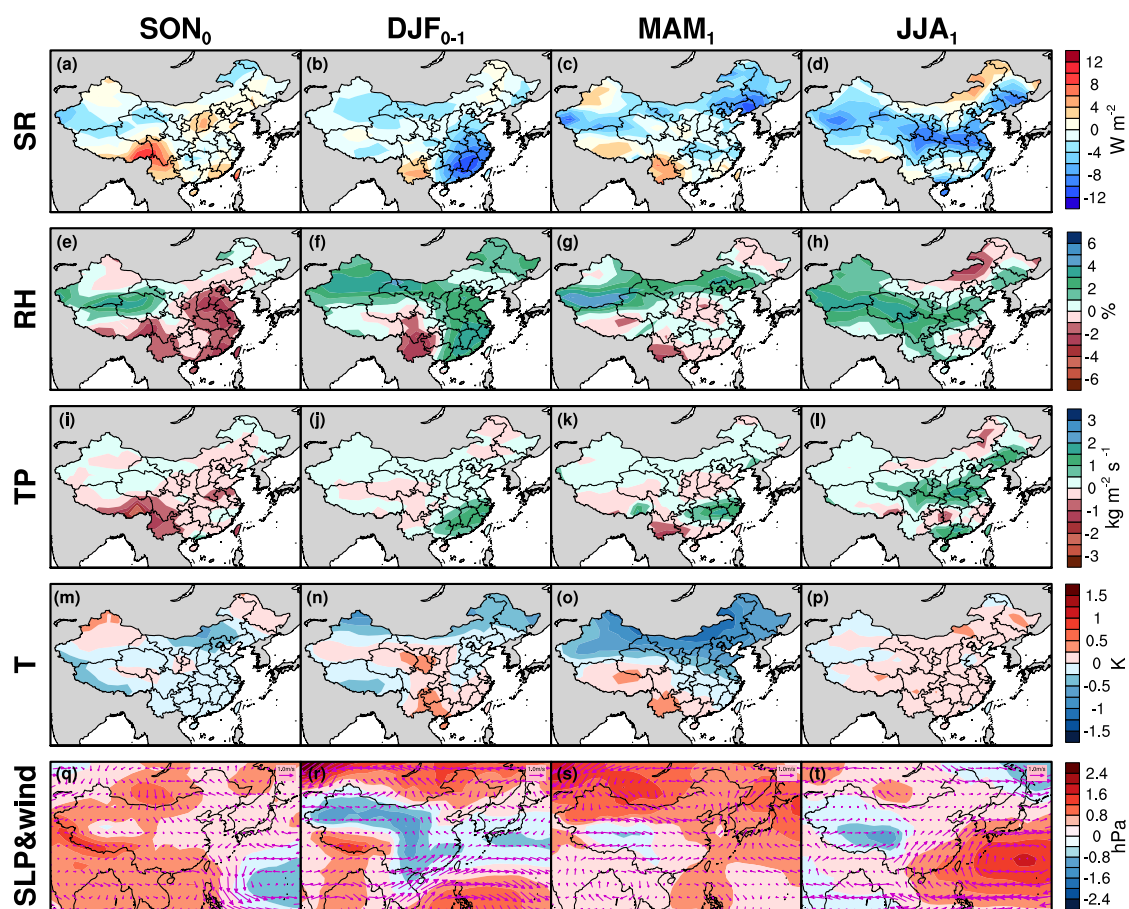


Figure 4. Same as Figure 3 except for CP El Niño.

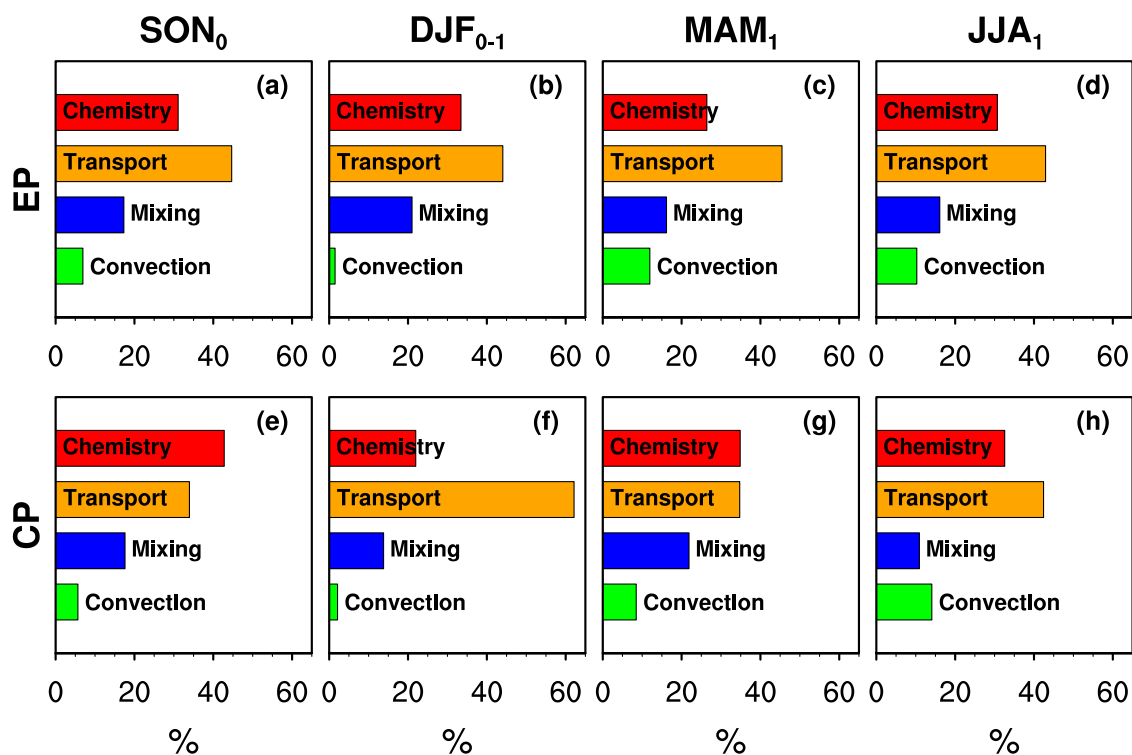


Figure 5. The absolute contribution (unit: %) of model processes, including chemistry, transport, mixing, and convection driven by the composite meteorological fields for four seasons in EP and CP El Niño years. These are the area-averaged values eastern China region (24.0–42.0°N, 100.0–117.5°E, purple box in Figure 6a).

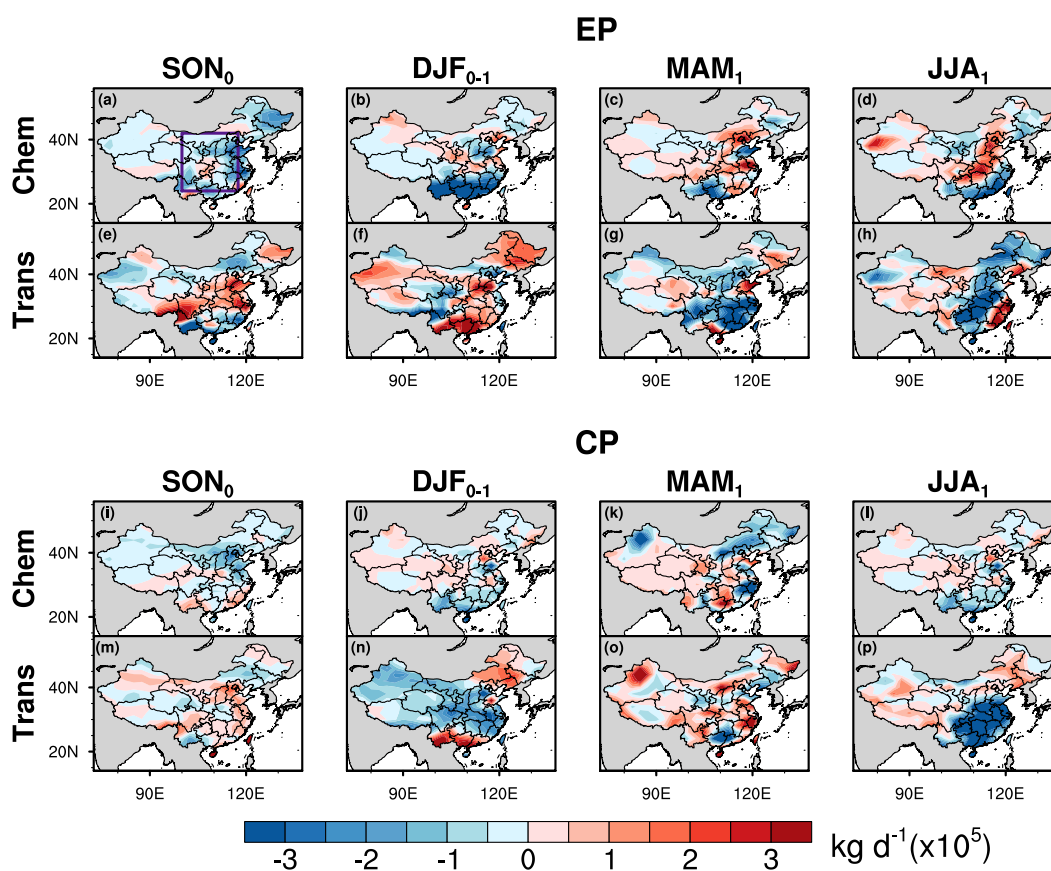


Figure 6. The composite tropospheric column ozone mass anomalies of chemistry and transport processes (0-6km, unit: kg d^{-1}) for four seasons in EP and CP El Niño years.



ONI-El Niño year	type		
	Niño3/4 method	EMI method	consensus
1982-1983	EP	EP	EP
1986-1987	/	EP	/
1987-1988	CP	EP	/
1991-1992	EP	CP	/
1994-1995	CP	CP	CP
1997-1998	EP	EP	EP
2002-2003	CP	CP	CP
2004-2005	CP	CP	CP
2006-2007	CP	EP	/
2009-2010	CP	CP	CP
2014-2015	/	CP	/
2015-2016	EP	EP	EP

Table 1. The classification results of EP and CP El Niño of the total 12 El Niño events from 1980 to 2017 using the Niño3/4 method and the EMI method.